OncoTargets and Therapy

Dovepress
open access to scientific and medical research

Open Access Full Text Article

ORIGINAL RESEARCH

Exploration of peptide T7 and its derivative as integrin αvβ3-targeted imaging agents

This article was published in the following Dove Press journal:
OncoTargets and Therapy
15 June 2015
Number of times this article has been viewed

Xin He[1]
Yumei Hao[1,2]
Wei Long[1]
Naling Song[1]
Saijun Fan[1]
Aimin Meng[1]

[1]Tianjin Key Laboratory of Radiation Medicine and Molecular Nuclear Medicine, Institute of Radiation Medicine, Peking Union Medical College and Chinese Academy of Medical Sciences, Tianjin, People's Republic of China; [2]Department of Reproductive Medicine, The Affiliated Hospital of Hebei University, Baoding, Hebei, People's Republic of China

Objective: The aim of the present study was to develop potential candidates of integrin αvβ3-targeted imaging agent, which can facilitate the diagnosis and treatment of malignant solid tumors.

Methods: Peptides derived from tumstatin, named T7 and T7-6H, were derivatized to contain histidine in the C-terminus of their sequence and were labeled with ^{99m}Tc via nitrido and carbonyl precursors. The radiochemical purity and stability of ^{99m}Tc-labeled T7 and T7-6H were characterized by thin-layer chromatography. The whole body biodistribution was studied in NCI-H157-bearing BALB/c nude mice.

Results: The ^{99m}Tc-labeled T7 and T7-6H showed adequate in vitro stability, with a high radiochemical purity of over 90%. The dissociation constant (Kd) value of the ^{99m}Tc-labeled T7 and T7-6H ranged from 68.5 nM to 140.8 nM in U251 and NCI-H157 cell lines. ^{99m}Tc-labeled T7 and T7-6H showed no significant difference of biodistribution in mice. Furthermore, both T7 and T7-6H exhibited a poor blood–brain barrier penetration and a transient accumulation in lung; the uptake in tumor tissues was significantly higher than in muscle tissue, with a ratio of 5.8.

Conclusion: ^{99m}Tc-labeled T7 and T7-6H can be regarded as promising single-photon emission computed tomography probes for imaging integrin αvβ3, and need to be further studied for noninvasive detection of tumors.

Keywords: integrin, angiogenesis, ligands

Introduction

It has been well known that angiogenesis plays an indispensable role in growth and metastasis of tumors since the idea was proposed by Folkman in 1971.[1] Integrin αvβ3, a member of the integrin family, also known as vitronectin receptor, has been most extensively studied as a crucial molecule during tumor angiogenesis.[2] Integrin αvβ3, a heterodimeric transmembrane glycoprotein consisting of αv (CD51, 150 kD) and β3 (CD61, 105 kD) subunits, is preferentially expressed in proliferating vascular endothelial cells and on surfaces of a wide variety of tumor cells including lung, breast, prostate cancer, osteosarcoma, neuroblastoma, and spongioblastoma cells. In contrast, in mature endothelial cells as well as the vast majority of normal tissues and organs, the integrin αvβ3 protein is undetectable or absent.[3] Therefore, integrin αvβ3 is a likely target for the diagnosis and therapy of tumors.[4]

A variety of extracellular matrix proteins combines with integrin αvβ3 via recognition of the Arg-Gly-Asp (RGD) sequence. Radio-labeled RGD peptides have been exploited as diagnostic radiopharmaceuticals. These radiopharmaceuticals can assess angiogenic activity of solid tumors, and monitor integrin-targeted antiangiogenic therapies.[5–7] A few researches also reveal that many ligands are able to bind to integrin αvβ3 in an RGD-independent way, such as SDV (Ser-Asp-Val) and SLV (Ser-Leu-Val).[8,9] In our previous studies,[10] we studied a peptide (T7) derived from tumstatin with the

Correspondence: Saijun Fan; Aimin Meng
Tianjin Key Laboratory of Radiation Medicine and Molecular Nuclear Medicine, Institute of Radiation Medicine, Peking Union Medical College and Chinese Academy of Medical Sciences, 238 Baidi Road, Nankai District, Tianjin, 300192, People's Republic of China
Email fansaijun@irm-cams.ac.cn; aiminmeng@irm-cams.ac.cn

sequence of Thr-Met-Pro-Phe-Leu-Phe-Cys-Asn-Val-Asn-Asp-Val-Cys-Asn-Phe-Ala-Ser-Arg-Asn-Asp-Tyr-Ser-Tyr-Trp-Leu (TMPFLFCNVNDVCNFASRNDYSYWL),[11–14] the results indicated that the binding specificity between T7 peptide and integrin αvβ3 is located at the active sites of Ser90, Arg91, Asp93, and Tyr94, a new non-RGD-dependent binding mode, namely RNDY binding mode. Other studies showed that the critical amino acid sites for anti-angiogenesis in T7 peptide were Leu78, Val82, and Asp84.[15] In the present study, we further explored the integrin binding capability of ^{99m}Tc-labeled T7 peptide and its derivative T7-6H in vitro and the biological distribution in vivo as potential radiotracers with high receptor-binding affinity/specificity in a noninvasive detection of tumor angiogenesis.

Materials and methods

General

In order to improve the hydrophilia without altering the activity and binding sites of T7, three hydrophobic amino acids within the C-terminus of the T7 sequence were replaced with three lysines (Lys, K). The modified T7 peptides were purchased from Beijing Scilight Biotechnology Led Co (Beijing, People's Republic of China) with a purity of 96.84% (high-performance liquid chromatography [HPLC], 220 nm; C18, linear gradient), molecular weight of 2,942.41; the sequence is TMPFLFCNVNDVCNFASRNDYSKKK. T7-6H was designed to obtain the more stable radio-labeled product by adding 6 histidine (His, H) into the C-terminus of the T7 sequence, ie, the T7 sequence was changed into TMPFLFCNVNDVCNFASRNDYSYWLHHHHHH, with a molecular weight of 3,843.29 and a purity of 99.32%.

All commercially obtained chemicals were of analytical grade and were used without further purification. Na $^{99m}TcO_4$ was obtained from a commercial ^{99}Mo/^{99m}Tc generator (Beijing Atom High Tech Co, Ltd, Beijing, People's Republic of China). The reversed phase HPLC system was fitted with a PLC column of Agela (250×4.6 mm ID) C18, detection wavelength of 220 nm. The thin-layer chromatography (TLC) scanner AR-2000 (Bioscan) was used to detect the radiochemical purity (RCP) of complexes.

Cell lines and cultures

Human breast cancer cells, MDA-MB-231 and MCF-7, were cultured in Dulbecco's Modified Eagle's Medium (DMEM) (Thermo Fisher Scientific, Waltham, MA, USA); human glioma cell line U251, human lung carcinoma cell line A549, human microvascular endothelial cell line HMEC-1, human esophageal cancer cell line EC109, laryngeal carcinoma cell line Hep2, human hepatocarcinoma cell line HepG2, human non-small cell lung cancer cell line NCI-H157, human lung cancer cell line NCI-H460, and prostate cancer cell line PC3 were maintained in Roswell Park Memorial Institute RPMI_1640 medium (Thermo Fisher Scientific). All media were supplemented with 10% fetal calf serum (Thermo Fisher Scientific), 10 U/mL penicillin, and 100 μg/mL streptomycin (Thermo Fisher Scientific). U251, EC109, Hep2, NCI-H157, and PC3 cell lines were obtained from the tumor cell library of the Peking Union Medical College (PUMC); MDA-MB-231, MCF-7, A549, HMEC-1, HepG2, and NCI-H460 cell lines were purchased from American Type Culture Collection (ATCC), Manassas, VA, USA.

Preparation and stability analysis of ^{99m}Tc-T7 and ^{99m}Tc-T7-6H

The preparation of ^{99m}Tc-T7 and ^{99m}Tc-T7-6H was carried out in two steps. Step one was the synthesis of the precursor fac-$[^{99m}Tc(CO)_3(H_2O)_3]^+$. $NaBH_4$ (20 mg), to which Na_2CO_3 (4 mg) and potassium sodium tartrate (15 mg) were added in a 10 mL glass vial. The vial was sealed, and a needle was introduced through the rubber stopper to equilibrate with the atmospheric pressure. CO gas was purged through the vial for 10 minutes, followed by an addition of 2.5 mL of saline containing $[^{99m}TcO_4]^-$ (activity ranging from 18.5 to 185 MBq). The vial was heated at 100°C for 15 minutes. The RCP of the precursor was evaluated by TLC. The TLC was performed on a polyamide strip with acetonitrile as mobile phase.

Synthesis of the ^{99m}Tc-T7 or ^{99m}Tc-T7-6H complex was the second step. The pH of the precursor fac-$[^{99m}Tc(CO)_3(H_2O)_3]^+$ was adjusted to 7 by adding 1 mol/L HCl solution and 0.5 mol/L phosphate buffer (pH 7.4). A water solution (1 mL) containing 1 mg of the T7 or T7-6H peptides was then added and kept for 30 minutes at room temperature. The RCP of the final complex was evaluated by using methods described previously in this section. The ^{99m}Tc-T7 or ^{99m}Tc-T7-6H was incubated at 37°C in saline or in rat serum separately; the RCP was assayed by TLC at different times after incubating for over 24 hours.

Flow cytometry

To determine the integrin αvβ3 expression levels in different cell lines, a flow cytometry assay was performed. Briefly, cells were collected and washed with phosphate-buffered saline (PBS) containing 1% bovine serum albumin (BSA). After blocking with 5% BSA in PBS, cells were incubated with an anti-CD51 + CD61 antibody [23C6], (1:20, ab93513; Abcam, Cambridge, UK) for 30 minutes at 4°C. After

washing with PBS containing 1% BSA, the cells were re-suspended in PBS, and were then analyzed using Accuri™ C6 (BD, Franklin Lakes, NJ, USA) with the 488 nm excitation wavelength and the 530 nm emission wavelength. The fluorescein isothiocyanate (FITC) signal intensity was analyzed using the Accuri™ C6 software (BD).

Cell binding kinetics of radio-labeled imaging agents

To quantitatively evaluate the binding affinities of ^{99m}Tc-T7 or ^{99m}Tc-T7-6H to the integrin αvβ3, an in vitro receptor binding and kinetics assay was carried out according to a radioactive ligand receptor binding assay method.[16,17] Cells were prepared at a 2×10^4 density in 500 μL medium per well in 24-well plates, separately. After incubation overnight, wells were washed with 500 μL pre-cooled PBS twice; non-specific binding wells were incubated with cold 80 mM T7 or T7-6H in 200 μL medium for 1 hour. Meanwhile, ^{99m}Tc-T7 or ^{99m}Tc-T7-6H was added to the specific binding wells at various concentrations: 5, 10, 20, 40, 80, and 160 nM, and were incubated for 1 hour at room temperature. Wells were washed with 500 μL pre-cooled PBS twice, were digested in 1 mL of 1 M NaOH, and finally, were measured by radioactive counter (SN-6100 automatic radioimmunoassay gamma counter, Hesuo Rihuan Photoelectric Instrument Co, Ltd, Shanghai, People's Republic of China). The dissociation constant (Kd) value was analyzed using a Scatchard method.

Animal models and biodistribution study

A subcutaneous NCI-H157 lung cancer model was established by subcutaneous injection of 6×10^6 cells suspended in 200 μL saline into the left flank of 6-week-old (17–19 g) female BALB/c nude mice. Mice were sacrificed for biodistribution and imaging studies when the tumor volume reached approximately 200–300 mm^3 (2–3 weeks after inoculation). All animals were numbered and kept separately in a temperature-controlled room on a 12-hour light/dark schedule with food and water ad libitum. All animal experiments were performed by licensed investigators in compliance with the national laws related to the conduction of animal experiments.

A solution (0.1 mL, 7.4 MBq) of the ^{99m}Tc-labeled peptides was administered via a tail vein to NCI-H157-bearing nude mice; the injected radioactivity was monitored with a gamma counter. Mice were sacrificed at 0.5, 1, 2, 4, and 8 hours following injection. Organs of interest and the blood were collected, wet-weighed, and measured for radioactivity detection. Results were expressed as percentage of the injected dose per gram of tissue (%ID/g). The radioactivity in each sample was calibrated against a known quantity of the injected dose. Values were expressed as means ± standard deviation (SD) (n=5).

Statistical analysis

All data were presented as mean values ± SD of at least three independent experiments. Student's *t*-test was applied with significance defined as $P<0.05$ (two-tailed test).

Results

Preparation and stability analysis of ^{99m}Tc-T7 and ^{99m}Tc-T7-6H

^{99m}Tc-T7 and ^{99m}Tc-T7-6H were synthesized by a two-step procedure, as described in the "Materials and methods" section. The extent of complexity was determined by TLC assay, where ^{99m}Tc-T7 and ^{99m}Tc-T7-6H exhibited a faster migration speed than $[^{99m}TcO_4]^-$ (Figure 1A); the RCP values of ^{99m}Tc-T7 and ^{99m}Tc-T7-6H were 92.1% and 91%, respectively (Figure 1B and C). The radio-labeled complex was injected intravenously, or was incubated in saline or rat serum to test the stability in vitro, with no need of further purification. The radio-labeled complexes containing ^{99m}Tc-T7 and ^{99m}Tc-T7-6H were observed to retain their RCPs to >90% after they had been stored 8 hours in saline or serum at 37°C (Figure 1D–G).

Integrin αvβ3 expression level of different cell lines

To qualify intrinsic αvβ3 integrin expression, flow cytometry analysis was performed using an FITC-labeled αvβ3 integrin-specific antibody in ten human cancer cell lines and one normal epithelial cell line (HMEC-1). As illustrated in Figure 2, the order for integrin αvβ3 expression was as follows: NCI-H157>U251>NCI-H460>A549>MCF-7>EC109>MDA-MB-231>HepG2>Hep2>PC3>HMEC-1, indicating a significantly higher αvβ3 integrin level in cancer cells than in HMECs.

Cell binding kinetics assay

In vitro receptor binding and kinetics assays were assessed in NCI-H157 and U251 cell lines according to the Scatchard diagram. No significant difference was observed for the Kd values of ^{99m}Tc-T7 and ^{99m}Tc-T7-6H in the same cell line, ie, 71.9 vs 68.5 nM in NCI-H157 cells, respectively ($P>0.05$), and 131.6 vs 140.8 nM in U251 cells, respectively ($P>0.05$). However, as shown in Figure 3, a significant difference in the Kd value of the same radio agent was observed, ie, 131.6 nM

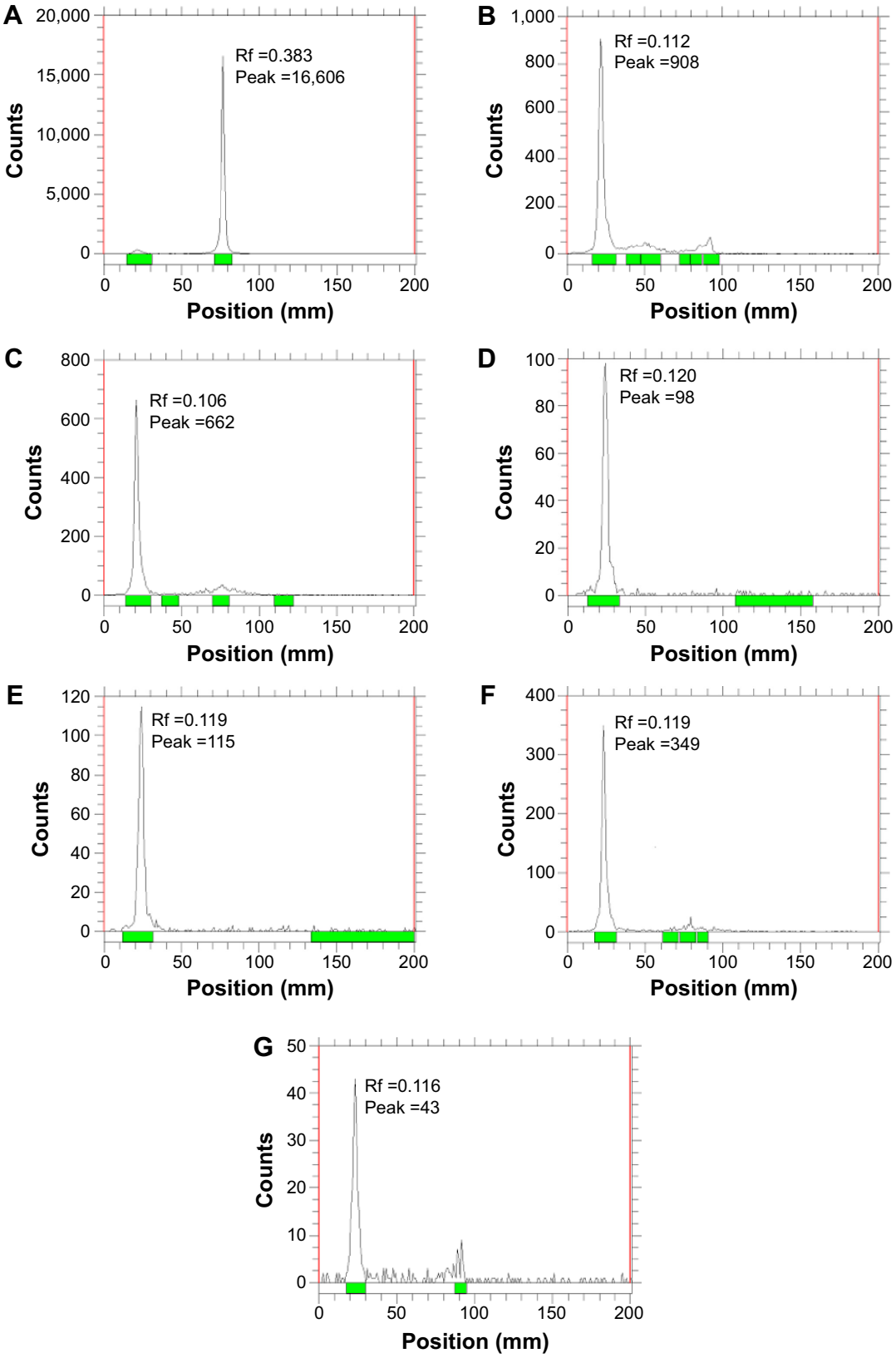

Figure 1 Radiochemistry and stability assay by TLC scan.
Notes: (**A**) [$^{99m}TcO_4$]$^-$, RCP =98%; (**B**) ^{99m}Tc-T7, RCP =92.1%; (**C**) ^{99m}Tc-T7-6H, RCP =91%; (**D**) ^{99m}Tc-T7 in saline for 8 hours at 37°C, RCP >90%; (**E**) ^{99m}Tc-T7 in serum for 8 hours at 37°C, RCP >90%; (**F**) ^{99m}Tc-T7-6H in saline for 8 hours at 37°C, RCP >90%; (**G**) ^{99m}Tc-T7-6H in serum for 8 hours at 37°C, RCP >90%. This experiment was repeated twice. The green shading in horizontal axis bar represents the peak positions.
Abbreviations: TLC, thin-layer chromatography; Rf, rate of flow.

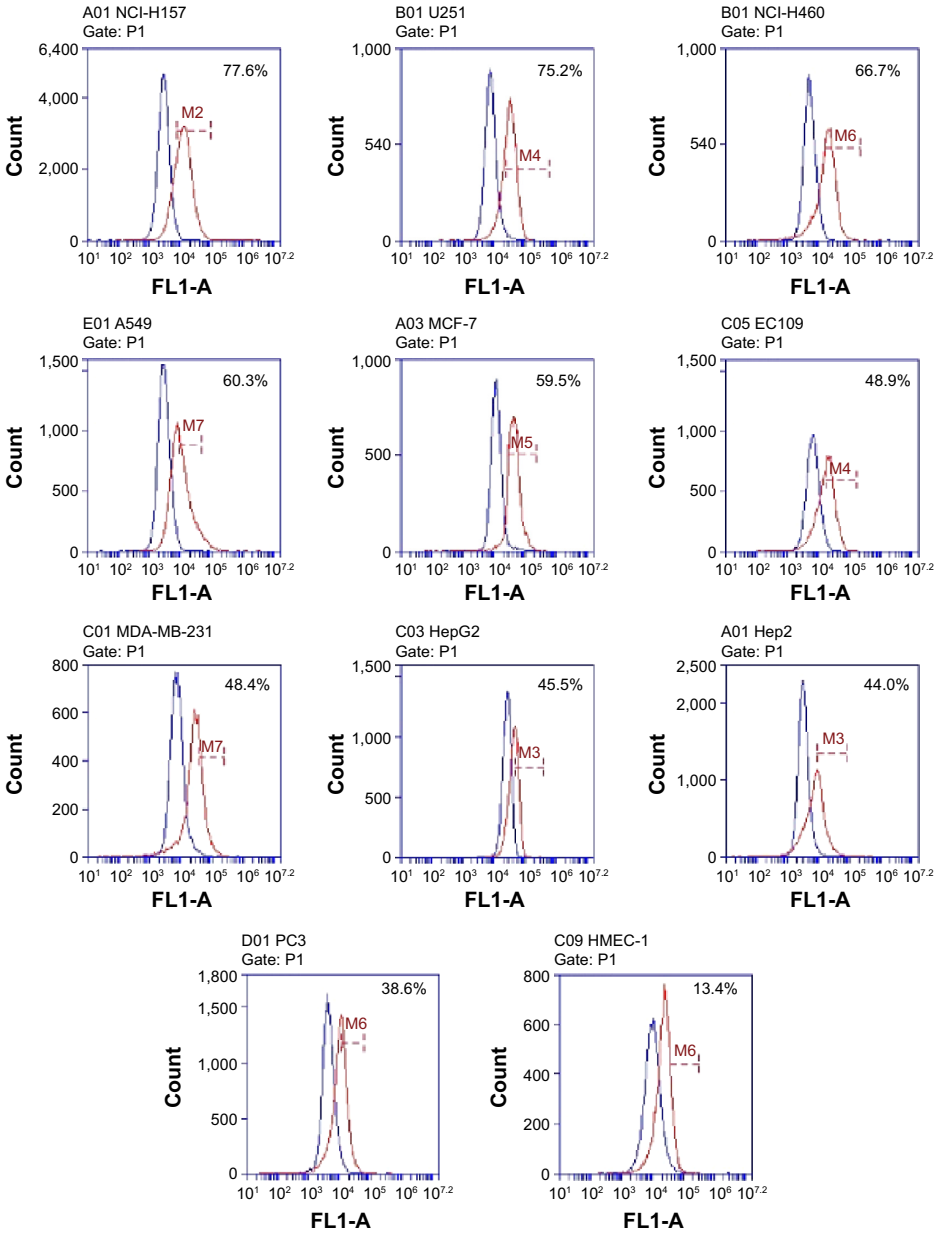

Figure 2 Flow cytometry analysis of integrin αvβ3 expression in eleven cell lines.
Note: This experiment was repeated twice.

in U251 cells vs 71.9 nM in NCI-H157 cells ($P<0.05$) for ^{99m}Tc-T7, and 140.8 nM in U251 cells vs 68.5 nM in NCI-H157 cells ($P<0.05$) for ^{99m}Tc-T7-6H. Taken together with the results in Figure 2, these findings suggest that, compared with amino acid sequence differences between T7 and T7-6H, the level of integrin αvβ3 expression may be more responsible for the binding affinity of radio agents.

In vivo biodistribution

Biodistributions of mice injected with ^{99m}Tc-T7 and ^{99m}Tc-T7-6H are summarized in Tables 1 and 2, and Figure 4. For example, a significantly high accumulation of ^{99m}Tc-T7 was observed in tumors at 0.0865±0.0023 %ID/g within 2 hours post-administration. Lung tissue bore the most accumulation of activity with 6.7260±0.1109 %ID/g within 2 hours post-administration, followed by liver with 2.3756±0.1085 %ID/g within 1 hour post-administration. However, the biodistribution in different organs/tissues was observed to diminish with time (Figure 4). The tumor/muscle ratio was found to slowly increase during the first 2 hours after injection, to reach maximum level at 2–4 hours post-administration. After 4 hours, the ratio started to decline with time.

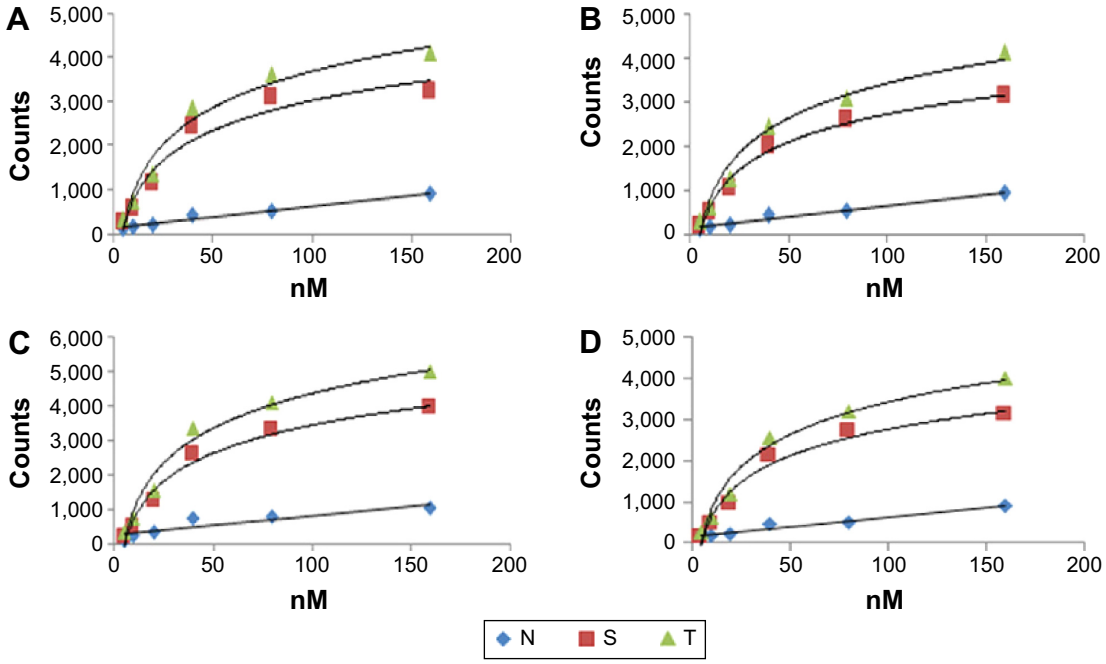

Figure 3 Saturation curve of ^{99m}Tc-labeled T7 and T7-6H binding with integrin αvβ3.
Notes: (**A**) ^{99m}Tc-T7 with U251, Kd =131.6 nM; (**B**) ^{99m}Tc-T7-6H with U251, Kd =140.8 nM; (**C**) ^{99m}Tc-T7 with NCI-H157, Kd =71.9 nM; (**D**) ^{99m}Tc-T7-6H with NCI-H157, Kd =68.5 nM.
Abbreviations: N, non-specific binding; S, specific binding; T, total binding.

The distribution values of ^{99m}Tc-T7 and ^{99m}Tc-T7-6H showed no significant difference in relation to selection of either complex as a candidate for tumor imaging (Tables 1 and 2, and Figure 4); these results suggested that the introduction of histidines into the C-terminal of T7 peptide does not alter its biological behavior. ^{99m}Tc-T7 or ^{99m}Tc-T7-6H showed a high accumulation in lung tissue. However, a weak accumulation was observed for both ^{99m}Tc-T7 and ^{99m}Tc-T7-6H in brain tissue, indicating that neither T7 nor T7-6H could penetrate the blood–brain barrier easily.

Discussion

The expression of αvβ3 integrin as a genuine marker of angiogenesis is only applicable to specific tumor types where its expression is restricted to vasculature; a key question in integrin imaging research is to what extent neovessel integrin expression contributes to radio-labeled imaging agents' binding capacity. Some aspects of T7 and integrin αvβ3 receptor behavior have been explored,[9,10,18] but in the context of diagnostic imaging, agents remain relatively underexplored. In the current study, we directly assessed the relationship of

Table 1 The biodistribution of ^{99m}Tc-T7 in the NCI-H157 model (%ID/g ± SD) (n=5)

Tissue	0.5 h	1 h	2 h	4 h	8 h
Heart	1.2931±0.0929	1.5536±0.1030	0.8279±0.0389	0.5147±0.0111	0.4377±0.0196
Liver	1.8305±0.0409	2.3756±0.1085	2.2373±0.1038	2.2010±0.0915	2.1768±0.0626
Spleen	2.0442±0.0460	2.2859±0.1238	1.8482±0.0580	1.5719±0.0609	1.4754±0.0748
Lung	3.4580±0.1132	6.6213±0.1688	6.7260±0.1109	3.2700±0.1049	2.7228±0.0551
Kidney	0.4919±0.0102	1.5367±0.1528	0.8617±0.0204	0.6673±0.0191	0.5370±0.0138
Muscle	0.0209±0.0012	0.0153±0.0007	0.0169±0.0008	0.0159±0.0008	0.0165±0.0007
Bone	0.0260±0.0022	0.0547±0.0022	0.0349±0.0013	0.0316±0.0010	0.0256±0.0003
Brain	0.0084±0.0005	0.0081±0.0002	0.0073±0.0003	0.0081±0.0006	0.0079±0.0001
Tumor	0.0256±0.0006	0.0359±0.0010	0.0865±0.0023	0.0785±0.0041	0.0737±0.0032
Blood	0.9284±0.0100	0.7706±0.0205	0.6692±0.0267	0.5530±0.0184	0.2459±0.0098
Intestine	0.0498±0.0011	0.0528±0.0034	0.0452±0.0021	0.0471±0.0012	0.0351±0.0018
Stomach	0.0862±0.0042	0.0880±0.0036	0.0775±0.0058	0.0773±0.0024	0.0719±0.0043

Abbreviations: h, hours; %ID/g, percentage of the injected dose per gram of tissue; SD, standard deviation.

Table 2 The biodistribution of ^{99m}Tc-T7-6H in the NCI-H157 model (%ID/g ± SD) (n=5)

Tissue	0.5 h	1 h	2 h	4 h	8 h
Heart	1.2931±0.0929	1.4936±0.0506	0.8679±0.0200	0.4927±0.0219	0.4577±0.0264
Liver	1.9205±0.0226	2.4376±0.0457	2.3159±0.1143	2.1855±0.0916	2.1768±0.0626
Spleen	2.1062±0.0726	2.2546±0.0475	1.9190±0.0437	1.6114±0.0824	1.3275±0.0390
Lung	3.5258±0.0767	6.4628±0.1051	6.7398±0.0812	3.4132±0.0659	2.6205±0.0776
Kidney	0.4527±0.0364	1.5552±0.1746	0.8636±0.0251	0.6567±0.0201	0.4590±0.0167
Muscle	0.0206±0.0011	0.0145±0.0003	0.0165±0.0007	0.0154±0.0006	0.0158±0.0006
Bone	0.0251±0.0015	0.0553±0.0026	0.0373±0.0010	0.0318±0.0008	0.0257±0.0010
Brain	0.0089±0.0002	0.0079±0.0002	0.0073±0.0003	0.0085±0.0005	0.0076±0.0002
Tumor	0.0308±0.0018	0.0389±0.0009	0.0889±0.0050	0.0831±0.0048	0.0792±0.0038
Blood	0.9286±0.0141	0.8602±0.0176	0.6630±0.0387	0.5664±0.0142	0.1634±0.0131
Intestine	0.0492±0.0037	0.0530±0.0031	0.0457±0.0028	0.0504±0.0028	0.0385±0.0036
Stomach	0.0815±0.0017	0.0802±0.0030	0.0787±0.0032	0.0824±0.0019	0.0790±0.0051

Abbreviations: h, hours; %ID/g, percentage of the injected dose per gram of tissue; SD, standard deviation.

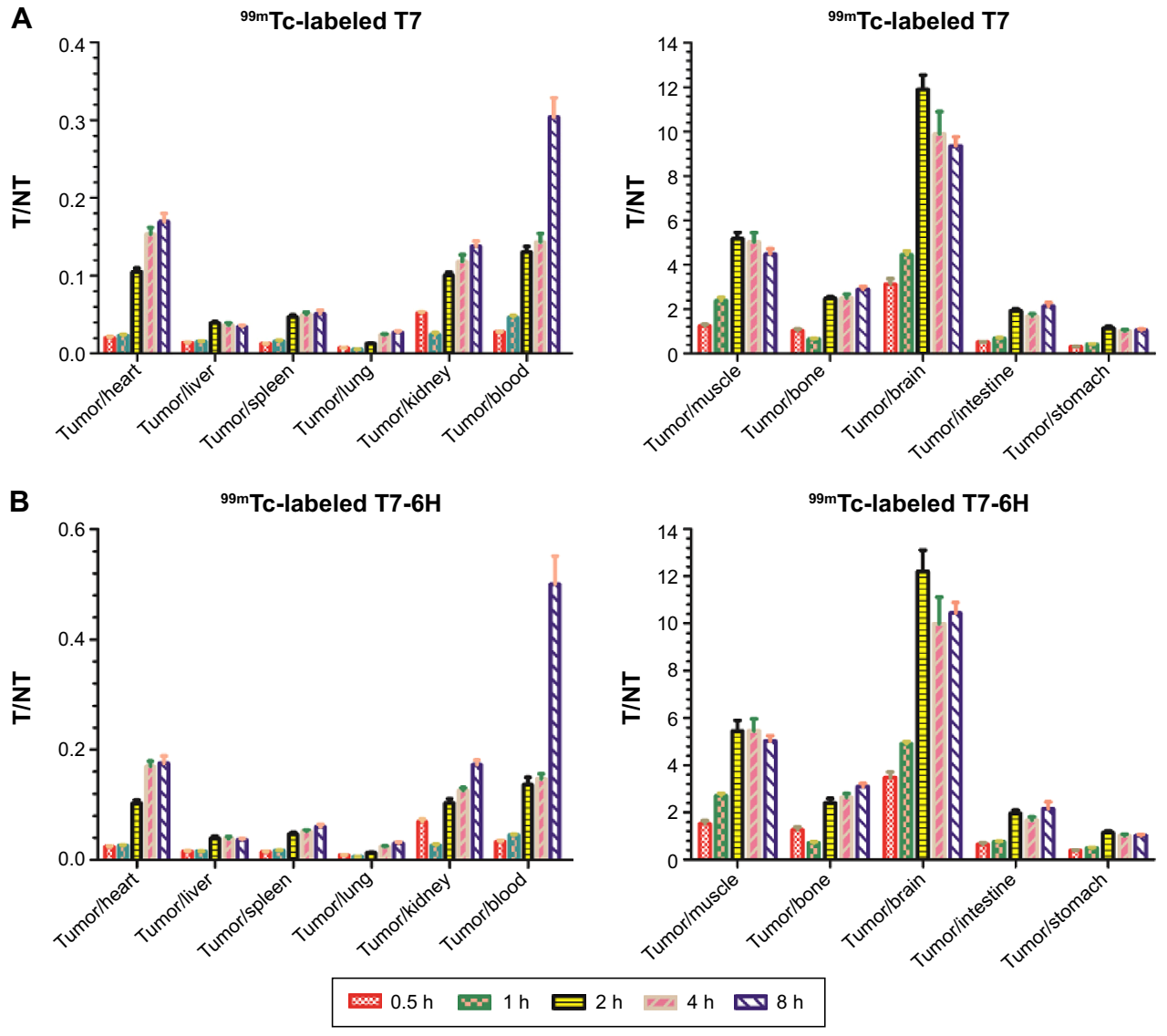

Figure 4 In vivo whole body biodistribution of ^{99m}Tc-T7 and ^{99m}Tc-T7-6H in NCI-H157-bearing nude mice model.
Notes: (**A**) The tumor/tissue ratios of ^{99m}Tc-T7; (**B**) the tumor/tissue ratios of ^{99m}Tc-T7-6H.
Abbreviations: h, hours; T/NT, tumor tissue/non-tumor tissue.

binding kinetics between T7 and T7-6H, with an introduction 6 histidine into the C-terminus of the T7 peptide, and an analysis of αvβ3 density in the in vitro cell lines and in vivo animal models. We used a two-step strategy with a product of >90% RCP, with no need for further purification. This radiochemical synthesis strategy worked well in our current experiments, because the reaction was not only fast enough for ^{99m}Tc labeling, but was also easily applied in labeling many different radioactive isotopes and large molecules with a precursor fac-[^{99m}Tc(CO)$_3$(H$_2$O)$_3$]$^+$.

In binding assays using a normal endothelial cell line and different kind of tumor cell lines, we confirmed that the ^{99m}Tc-labeled probe binding kinetics as shown with the Kd value, varied broadly with the integrin αvβ3 expression levels in the cell lines (Figures 2 and 3). ^{99m}Tc-labeled T7 and T7-6H occupied the specific binding sites of integrin αvβ3, because non-specific binding was excluded by using cold competing peptide. However, ^{99m}Tc-labeled T7 and T7-6H showed no significant differences in binding affinity, which reflects the fact that the key amino acid residues of T7 that interact with integrin αvβ3 receptor are not affected, in accordance with our previous results.[10]

The results from the in vitro receptor binding and kinetics assay (Figure 3) are not consistent with the αvβ3 integrin expression profiles obtained using FCM (Figure 2). Expression of αvβ3 integrin was similar for both NCI-H157 and U251 cell lines using FCM. However, the Kd values using the same peptide were dramatically different for these different cell lines. It has been demonstrated previously that the αvβ3 integrin binds to RGD peptides in its activated state, where the receptor adopts an open conformation.[19] Quantification of αvβ3 expression on the surface of eleven different cell lines was performed by FCM using antibody (ab93513; Abcam), which was monocloned based on the RGD recognizing mode (as per Abcam's product description); however, in the current research, T7 or T7-6H bound to αvβ3 integrin in a different way, which may provide an explanation for the discrepancy between FCM results and Kd values. It also indicated that non-RGD binding mode may have a stronger correlation, specifically between αvβ3 integrin and the tracer, than RGD binding mode. At this point, mathematical approaches should be used to assess this phenomenon.

In vivo distribution data revealed that the ^{99m}Tc-labeled T7 and T7-6H peptides exhibited friendly potential as noninvasive imaging probes, because of the significantly high tumor uptake of 0.0865±0.0023 %ID/g within 2 hours post-administration and the relatively high tumor/muscle ratio. However, the biodistribution and accumulation of both T7 and T7-6H peptides varied among non-target organs, eg, distribution/accumulation was low in the intestine and high in the lung. There were many factors affecting the tracer uptake, including probe specificity, hydrophilicity, metabolism, penetrating ability, and so on. Zhang et al[20] reported similar observations; many tumor cells grown in culture did not reflect the levels of integrin in tumor tissue of the model. Considering of the probes' properties (yield, stability, and absorption) overall, and taking into account integrin expression, the interpretation of tracer distribution and its kinetic parameters should be evaluated in more detail. It is well documented that αvβ3 integrin is not only restricted to a variety of tumor cells, but also that its high expression occurs on the surface of vessels during angiogenesis.[5,6,21] In the last decade, noninvasive imaging of αvβ3 integrin using RGD peptides, including radiotracers, has been extensively investigated for diagnosing cancer and other disorders and for monitoring treatment response,[22,23] and have been used in a clinical trial.[23] Our previous studies focus on a non-RGD binding mode peptide[10,12] may provide a promising approach in obtaining more comprehensive and complementary disease information via one-step examination procedures, with easy availability and low cost.

In consideration of the important role integrin αvβ3 plays in many pathological and physiological processes, especially in cancer and fibrosis, noninvasive imaging of integrin αvβ3 expression would provide a great deal of information to benefit disease detection, new drug development and validation, and patient management (eg, treatment monitoring and dose optimization).[24–27] Quantitative correlation of probe uptake with integrin αvβ3 expression level, as demonstrated in the current research on ^{99m}Tc-labeled T7 and T7-6H, would facilitate the development of noninvasive tests and personalized treatment.

We recognize several potential limitations of our current study; it would be interesting to perform a side-by-side comparison of the two types of radiotracers (RGD and non-RGD) in the same cell line and same animal by measuring Kds and biodistribution.

Conclusion

In summary, two novel water-soluble αvβ3-targeting agents, T7 and T7-6H, were designed and synthesized. Probes were radio-labeled with ^{99m}Tc, obtained from a commercial ^{99}Mo/^{99m}Tc generator, with high RCP. ^{99m}Tc-labeled T7 and T7-6H were found to be quite hydrophilic and exhibited adequate stability in vitro as well as in rat serum. Preliminary biological evaluation carried out in BALB/c nude mice bearing NCI-H157 heterotopic lung tumors revealed significant uptake and retention of ^{99m}Tc-labeled T7 and T7-6H in the

tumor compared to normal tissues. The non-target uptake observed at initial time points gradually decreased with time, which was reflected in the improved tumor-to-blood and tumor-to-muscle ratios that were achieved at the later time points. The present experiments indicate a potential application of ^{99m}Tc-labeled T7 as a single-photon emission computerized tomography radiotracer for tumor imaging.

Acknowledgments

The authors are thankful to Professor Tan Jian, director of the Nuclear Medicine Department, Tianjin Medical University General Hospital; and Jianfeng Liu and Dezhi Wang, Tianjin Key Laboratory of Radiation Medicine and Molecular Nuclear Medicine, for their support. The current work was funded by PUMC Youth Fund (grant number 2012J06) and the Development Fund of the Institute of Radiation Medicine (IRM) (grant number SF1306 and SF1418).

Disclosure

The authors report no conflicts of interest in this work.

References

1. Folkman J. Tumor angiogenesis: therapeutic implications. *N Engl J Med*. 1971;285(21):1182–1186.
2. Brooks PC, Clark RA, Cheresh DA. Requirement of vascular integrin αvβ3 for angiogenesis. *Science*. 1994;264(5158):569–571.
3. Max R, Gerritsen RR, Nooijen PT, et al. Immunohistochemical analysis of integrin alpha vbeta3 expression on tumor-associated vessels of human carcinomas. *Int J Cancer*. 1997;71(3):320–324.
4. Liu Z, Wang F, Chen X. Integrin αvβ3-targeted cancer therapy. *Drug Dev Res*. 2008;69(6):329–339.
5. Liu Z, Wang F. Development of RGD-based radiotracer for tumor imaging and therapy: translating from bench to besides. *Curr Mol Med*. 2013;13(10):1487–1505.
6. Li Y, Liu Z, Dong C, et al. Noninvasive detection of human-induced pluripotent stem cell (hiPSC)-derived teratoma with an integrin-targeting agent (99m)Tc-3PRGD2. *Mol Imaging Biol*. 2013;15(1):58–67.
7. Alam IS, Witney TH, Tomasi G, et al. Radiolabeled RGD tracer kinetics annotates differential αvβ3 integrin expression linked to cell intrinsic and vessel expressions. *Mol Imaging Biol*. 2014;16(4):558–566.
8. Choi Y, Kim E, Lee Y, Han MH, Kang IC. Site-specific inhibition of integrin αvβ3-vitronectin association by a Ser-Asp-Val sequence through an Arg-Gly-Asp-binding site of the integrin. *Proteomics*. 2010;10(1):72–80.
9. Liu Y, Yang Y, Zhang C. A concise review of magnetic resonance molecular imaging of tumor angiogenesis by targeting integrin αvβ3 with magnetic probes. *Int J Nanomedicine*. 2013;8:1083–1093.
10. Zan J, He X, Long W, Liu P. Insights into binding modes of tumstatin peptide T7 with the active site of αvβ3 integrin. *Mol Simulat*. 2012;38:498–508.
11. Maeshima Y, Colorado PC, Torre A, et al. Distinct antitumor properties of a type IV collagen domain derived from basement membrane. *J Biol Chem*. 2000;275(28):21340–21348.
12. Maeshima Y, Colorado PC, Kalluri R. Two RGD-independent alpha v beta 3 integrin binding sites on tumstatin regulate distinct anti-tumor properties. *J Biol Chem*. 2000;275(31):23745–23750.
13. Petitclerc E, Boutaud A, Prestayko A, et al. New functions for non-collagenous domains of human collagen type IV. Novel integrin ligands inhibiting angiogenesis and tumor growth in vivo. *J Biol Chem*. 2000; 275(11):8051–8061.
14. Maeshima Y, Yerramalla UL, Dhanabal M, et al. Extracellular matrix-derived peptide binds to alpha(v)beta(3) integrin and inhibits angiogenesis. *J Biol Chem*. 2001;276(34):31959–31968.
15. Eikesdal HP, Sugimoto H, Birrane G, et al. Identification of amino acids essential for the antiangiogenic activity of tumstatin and its use in combination antitumor activity. *Proc Natl Acad Sci U S A*. 2008;105(39): 15040–15045.
16. Maguire JJ, Kuc RE, Davenport AP. Radio ligand binding assays and their analysis. In: *Receptor Binding Techniques*. New York: Humana Press; 2005:18–19,101–102,121–122,203–204.
17. Davenport AP, Russel FD. Radio ligand binding assays: theory and practice. In: Mather SJ, editor. *Current Directions in Radiopharmaceutical Research and Development*. Amsterdam: Springer Netherlands; 1996:169–179.
18. Grafton KT, Moir LM, Black JL, et al. LF-15 and T7, synthetic peptides derived from tumstatin, attenuate aspects of airway remodelling in a murine model of chronic OVA-induced allergic airway disease. *PLoS One*. 2014;9(1):e85655.
19. Takagi J, Petre BM, Walz T, Springer TA. Global conformational rearrangements in integrin extracellular domains in outside-in and inside-out signaling. *Cell*. 2002;110(5):599–611.
20. Zhang X, Xiong Z, Wu Y, et al. Quantitative PET imaging of tumor integrin alphavbeta3 expression with 18F-FRGD2. *J Nucl Med*. 2006; 47(1):113–121.
21. Gaertner FC, Kessler H, Wester HJ, Schwaiger M, Beer AJ. Radiolabelled RGD peptides for imaging and therapy. *Eur J Nucl Med Mol Imaging*. 2012;39(Suppl 1):S126–S138.
22. Schottelius M, Laufer B, Kessler H, Wester HJ. Ligands for mapping alphavbeta3-integrin expression in vivo. *Acc Chem Res*. 2009; 42(7): 969–980.
23. Liu Z, Wang F. Development of RGD-based radiotracers for tumor imaging and therapy: translating from bench to bedside. *Curr Mol Med*. 2013;13(10):1487–1505.
24. Haubner R, Wester HJ, Burkhart F, et al. Glycosylated RGD-containing peptides: tracer for tumor targeting and angiogenesis imaging with improved biokinetics. *J Nucl Med*. 2001;42(2):326–336.
25. Battle MR, Goggi JL, Allen L, Barnett J, Morrison MS. Monitoring tumor response to antiangiogenic sunitinib therapy with 18F-fluciclatide, an 18F-labeled αVbeta3-integrin and αV beta5-integrin imaging agent. *J Nucl Med*. 2011;52(3):424–430.
26. Terry SY, Abiraj K, Frielink C, et al. Imaging integrin αvβ3 on blood vessels with 111In-RGD2 in head and neck tumor xenografts. *J Nucl Med*. 2014;55(2):281–286.
27. Ji S, Zhou Y, Voorbach MJ, et al. Monitoring tumor response to linifanib therapy with SPECT/CT using the integrin αvβ3-targeted radiotracer 99mTc-3P-RGD2. *J Pharmacol Exp Ther*. 2013;346(2):251–258.